Voyager Evidence for Large-Scale Spatial Structure in Plasma and Particle Behavior Beyond the Termination Shock

D S Intriligator[1], W D Miller[1], J Intriligator[1,2], and W Webber[3]
[1]Carmel Research Center, Inc., Santa Monica, CA
[2]Tufts University, Medford, MA
[3]New Mexico State University, Las Cruces, NM

E-mail: devriei@aol.com

Abstract. Voyager 1 crossed the termination shock at the end of 2004, more than a full solar cycle ago. Similarly, Voyager 2 crossed it and entered the heliosheath at the end of August, 2007, which was before the beginning of SC 24. Voyager 1 crossed the heliopause in August, 2012, when solar activity was high. Thus, at each spacecraft changing readings over time in the heliosheath could be due either to the increasing solar distance or to changing solar activity. Comparing observations by the two spacecraft at corresponding distances shows cases for which distance is more important. In particular, at both spacecraft the spectral index of protons in the anomalous cosmic ray energy range shows corresponding variations with distance, despite the differing times and the great separation between the spacecraft, and so do ratios of electron count rates in differential energy bands. These comparisons provide insight into the expectation that Voyager 2 will soon cross the heliopause. Consideration of the large-scale spatial structure of moving flare-generated disturbances also provides insight into particle behaviour associated with the plasma wave events observed by Voyager 1 since it crossed the heliopause. We discuss a variety of observations of these phenomena from the heliosheath and the local interstellar medium and suggest a possibility for future simulations.

1. Introduction

As Voyagers 1 and 2 (V1 and V2) continue ever farther from the Sun, their measurements of space environment conditions not observable from the Earth pose continuing challenges of coherently understanding them. The heliographic inertial latitude of the trajectory of V1 is about 34 degrees north, while the latitude of the trajectory of V2 is about 30 degrees south, and they are also separated by nearly 45 degrees in longitude. Thus, the distance between the two spacecraft is of the same order of magnitude as their respective distances from the Sun, although at a solar distance of nearly 142 AU, V1 is now significantly farther from the Sun than V2 is at more than 117 AU.

For a number of years, we analyzed understanding various physical phenomena associated with the Voyager data. We followed the Halloween 2003 events from the Sun to Earth, Ulysses, Cassini, and the Voyagers [1-3]. We also followed a number of other specific events from the Sun to the Voyagers e.g., July 2012 [4]. Without the Ulysses data these events are more difficult to follow across the heliosphere. V1 has been in the local interstellar medium (LISM) for more than 5 years, but the V1 plasma instrument (PLS) has not worked since 1980. Since then the only available estimates of the plasma environment at V1 have come from when they were inferred indirectly using data from the Low Energy Charged Particle (LECP) instrument (Decker [5]). Recently we have used the V1 Cosmic Ray System (CRS) (Stone [6]) for similar inferences. However, the V2 PLS is still working well enough that it is expected to be able to make direct observations of the LISM plasma after the heliopause (HP) is crossed, so there is great interest in when this will happen. V1 crossed the HP in August, 2012 (Webber and McDonald; Stone, et al. [7]), near 121.7 AU from the Sun. If the HP near V2's trajectory is at the same distance, then the HP crossing is still more than a year away. Webber and Intriligator [8] implied that V2 may see the HP in the South at a radial distance of ~10 AU closer than that observed at V1. However, assuming that the LISM particle environment near V2's trajectory is similar to that near V1's trajectory implies that comparing the histories of particle data in the heliosheath on V1 and V2 may provide insights into the approach to the HP. Evidently, these comparisons also provide insight into conditions in the heliosheath. On the other hand, data from V1

since the HP crossing show that the behavior of particles in the LISM is more complex than previously expected, because the strongest interplanetary disturbances generated by solar flares propagate all the way through the heliosheath and out into the LISM, where they generate plasma wave events as well as perturbing particle propagation. This complex behavior needs to be studied further.

Thus, the results we present here go substantially beyond our recent studies [9,10] connecting major flares of SC 24 with events in the heliosheath and LISM. We describe evidence that the electron spectrum observed by the V1 CRS changed very little at the HP, despite the relatively large change in count rates, and that the electron spectrum observed by the V2 CRS is now closely similar to the V1 spectrum near and beyond the HP, implying that the crossing may be near. We also compare these data with CRS proton data in the anomalous cosmic ray (ACR) energy range and discuss how these analyses might be affected by particle effects associated with plasma wave events generated by interplanetary disturbances generated by solar flares as they propagate out into the LISM.

2. Differential Electron Energy Bands

As described in more detail at the Voyager CRS website [11], the telescopes of the CRS consist of stacks of solid-state detectors, mounted so that particles can enter either end of each stack, with a guard detector surrounding each stack and coincidence logic incorporated into the data system. This logic identifies simultaneous energy deposition events in various combinations of detectors and thereby distinguishes counts caused by electrons from counts caused by positive ions. Among positive ions, it discriminates between protons, alpha particles, and heavier nuclei, as long as the guard detector is not triggered. Triggering this detector indicates that a particle came through the side of the telescope instead of from the desired field of view; thus readings from other detectors would be an incomplete or mistaken characterization of the particle, and are therefore rejected. The data system also reports for each accepted event how much energy was deposited in each detector, but the rates page of the website [11] only lists count rates for various types of events, including not only coincidence events but also count rates in individual detectors, without including energy information.

The CRS has two high-energy telescopes, designated HET-I and HET-II, which are identical except for being mounted with their fields of view in different directions. These telescopes have detector coincidences that count both ions and electrons, and in particular there are coincidence combinations that identify electrons that stop in detector C4 of the HET: electrons with higher energies that penetrate C4 but stop in C3; and electrons with still higher energies that penetrate both C4 and C3, but stop in C2. Figures 1(a), 1(b), and 1(c) show the time series of the count rates for the respective detectors of HET-I on V1 from the beginning of 2004 to the end of 2017. (The corresponding plots for HET-II are so nearly identical that they are not shown.)

Although these histories look similar during most of this period of 14 years, with the HP crossing emphatically evident in all of them, the C4 plot in Figure 1(a) shows a small peak around the time of the TS crossing at the end of 2004 that has little if any counterpart in Figures 1(b) and 1(c). Thus, for a clearer comparison the C4/C3 and C3/C2 ratios were calculated and are shown in Figures 1(d) and 1(e). Figure 1(d) evidently shows not only a prominent brief peak in the C4/C3 ratio around the TS crossing but also a longer subsequent period of ratios (around 8) that then gradually decline to around 4 (indicating that this portion of the spectrum became harder) while Figure 1(e) shows very little evidence of a peak near the TS crossing, but a gradual rise in the C3/C2 ratio from around 2.0, with a great amount of scatter, to between 2.5 and 3.0 with less scatter. However, despite the sharp rises in the individual count rates at the HP crossing, neither ratio plot shows a visible change then, suggesting that the electrons observed in these energy bands in the heliosheath as the spacecraft was approaching the HP may have diffused inward from the LISM.

Thus, Figures 2(a) through 2(e) show the corresponding time series for HET-I of the V2 CRS, which is the only high-energy telescope on V2 on which these coincidence counters still function. Each part of Figure 2 is plotted on the same scale as the corresponding part of Figure 1 to aid comparisons.

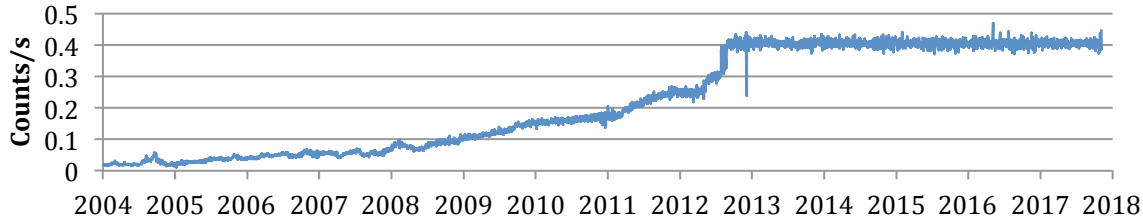

Figure 1(a). Count rate of electrons stopping in detector C4 of HET-I of the V1 CRS.

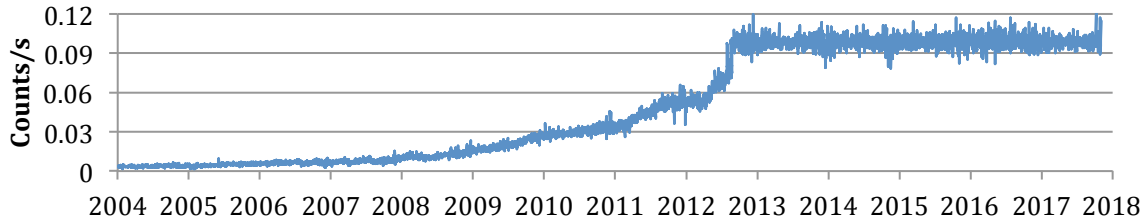

Figure 1(b). Count rate of electrons stopping in detector C3 of HET-I of the V1 CRS.

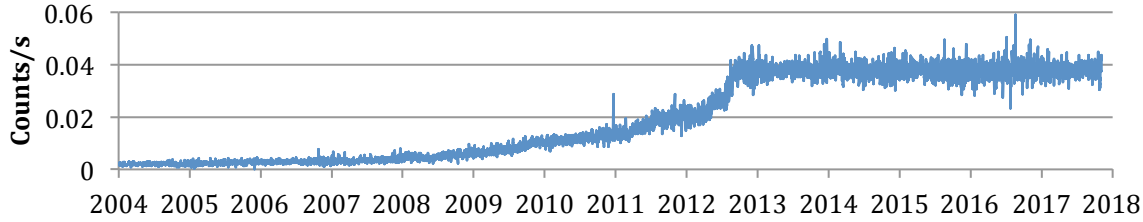

Figure 1(c). Count rate of electrons stopping in detector C2 of HET-I of the V1 CRS.

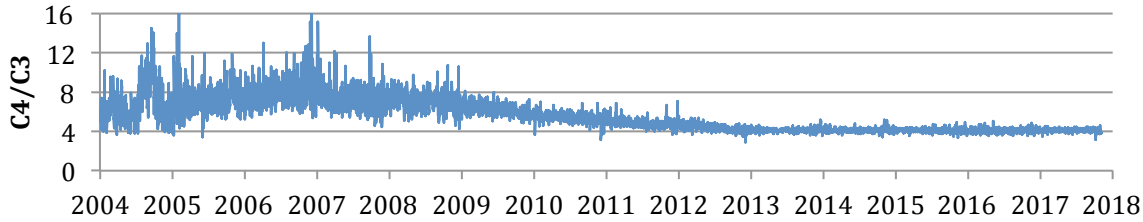

Figure 1(d). C4/C3 count rate ratio for HET-I of the V1 CRS.

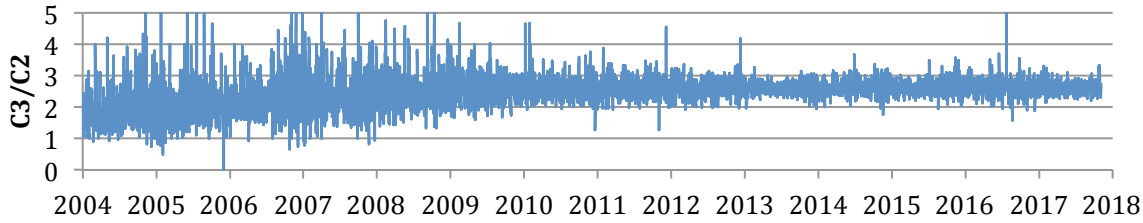

Figure 1(e). C3/C2 count rate ratio for HET-I of the V1 CRS.

Comparing Figure 1 with Figure 2 shows that as of the most recent data in late 2017 the V2 count rates in Figures 2(a), 2(b), and 2(c) were approximately the same as the corresponding V1 count rates in late 2011 in Figures 1(a), 1(b), and 1(c). Furthermore, the V2 ratios in Figures 2(d) and 3(e) show the same trends as the V1 ratios in Figures 1(d) and 1(e) (C4/C3 downward toward 4 and C3/C2 upward toward 2.5) and by late 2017 were approximately the same as the corresponding V1 ratios

were in late 2011. This may be more significant than the correspondence of the count rates, because using the ratios compensates for the possibility that the count rates at the HP may be different for V2.

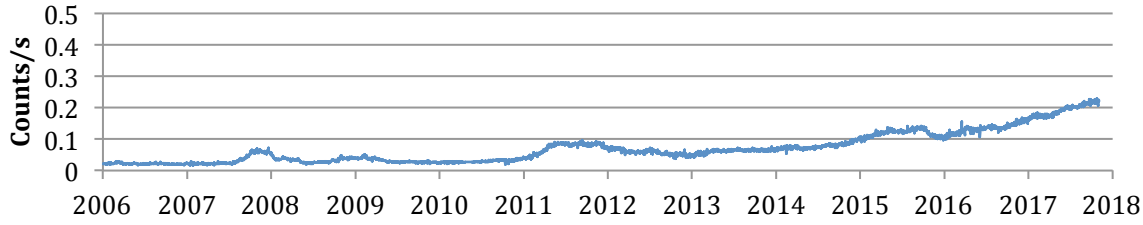

Figure 2(a). Count rate of electrons stopping in detector C4 of HET-I of the V2 CRS.

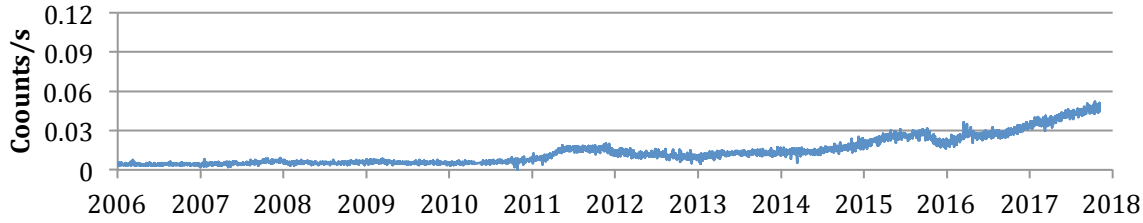

Figure 2(b). Count rate of electrons stopping in detector C3 of HET-I of the V2 CRS.

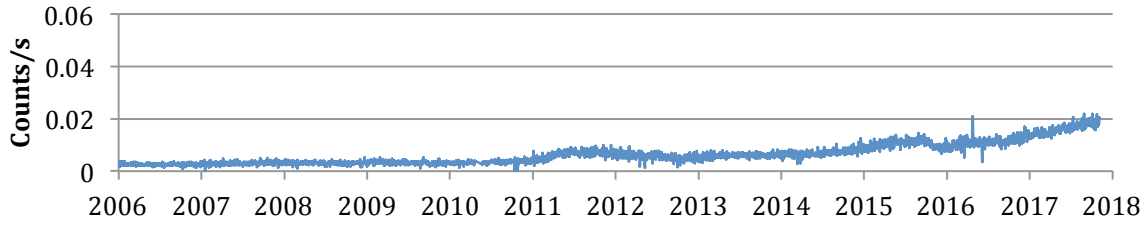

Figure 2(c). Count rate of electrons stopping in detector C2 of HET-I of the V2 CRS.

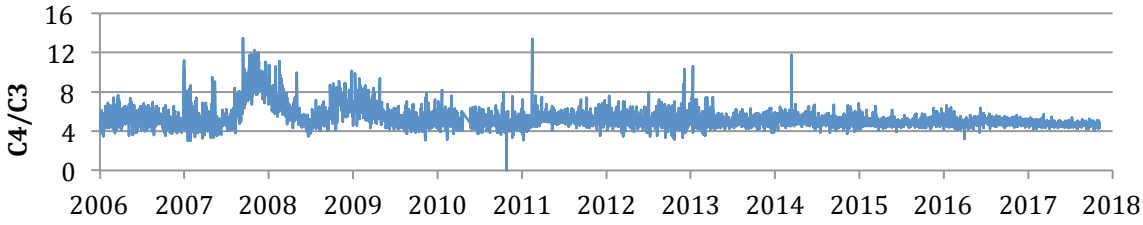

Figure 2(d). C4/C3 count rate ratio for HET-I of the V2 CRS.

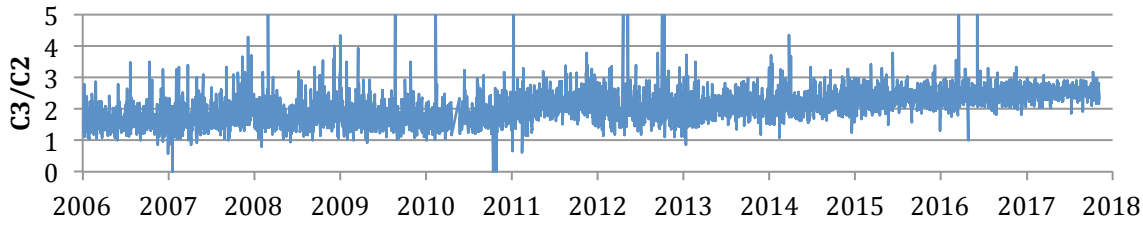

Figure 2(e). C3/C2 count rate ratio for HET-I of the V2 CRS.

This could happen if, for example, Opher, et al. [12] are correct that beyond the TS the fluctuations in the heliospheric current sheet (HCS) are compressed by the deceleration of the solar wind until portions of the HCS reconnect to form a disordered structure of magnetic islands and bubbles. This

reconnection would accelerate anomalous cosmic rays and energetic electrons and the magnetically disordered plasma would interact with the LISM to produce a north-south asymmetry between the electron intensities at V1 and V2, with energetic electrons being locally trapped in the islands and bubbles. They performed a high-resolution 3-D MHD simulation predicting that the LISM field is stronger on the south side of the nose of the heliosphere and would therefore have higher pressure. This would cause most of the islands and bubbles to be carried to the northern hemisphere. Then the TS in the south would be closer to the Sun than in the north, consistent with the Voyager TS crossings at 94 AU in the north and 84 AU in the south [8]. Having fewer magnetic islands and bubbles in the south would allow easier diffusion of energetic electrons in this region, so that when V2 reaches the HP it may not see the steep rise in electron count rates observed at V1, as shown in Figures 1(a) - 1(c). Another possibility is that the LISM ahead of the heliosphere is like the simulations of Pogorelov, et al. and of Borovikov and Pogorelov [13], who predict a lumpy and rippled HP due to the Rayleigh-Taylor and Kelvin-Helmholtz instabilities, resulting in irregular compression of the LISM near the HP.

However, it remains to be seen whether the results of the simulation in [12] are consistent with the work in [14]. As we noted last year, it combined Voyager LECP observations and energetic neutral atom (ENA) data from Cassini to estimate the thickness of the heliosheath in the direction of V2. This work updated estimates originally made for V1 and V2 in 2010 in [15], in which the thickness for V1 was estimated at around 30 AU and for V2 was estimated as at least 40 AU. As the actual thickness observed by V1 was about 27.7 AU and V2 has now travelled nearly 34 AU through the heliosheath without reaching the HP (though it may be close), the ENA estimates appear to have been sufficiently reliable thus far that they may deserve additional comparisons with estimates made by other methods.

3. Proton Spectral Indices in the ACR Energy Range in the Heliosheath

As the ratio plots in Figures 1 and 2 imply that electron energy spectra in the heliosheath change with distance, this naturally raises the question of corresponding changes in positive ion energy spectra. The V1 and V2 pages of the COHO website include 6-hour and daily averages of CRS proton fluxes in 8 adjacent energy bands from 3.4 to 56.0 MeV. Example plots of the logarithms of these fluxes versus the logarithms of the energies of the midpoints of the energy bands showed approximately straight lines with substantial changes of slope over time in the heliosheath for both spacecraft, with the spectra soon after the TS crossing being substantially softer than those of particles observed later.

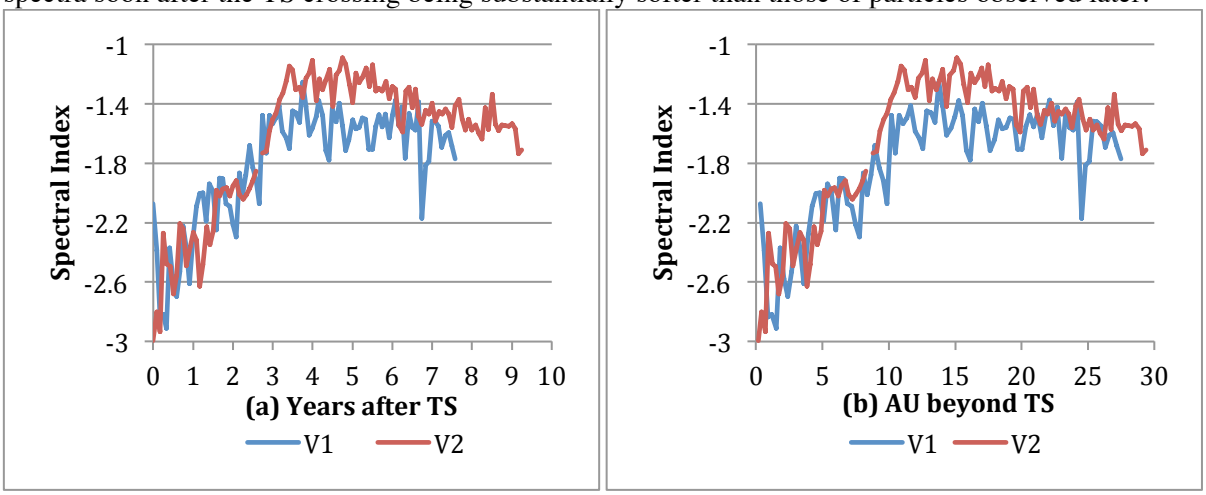

Figure 3. Spectral indices of monthly samples of CRS protons from 3.4 to 56.0 MeV at V1 and V2 as functions of (a) time after crossing the TS and (b) distance beyond the TS.

For a more comprehensive view of this behavior, a monthly sample spectrum from the middle day of each month was taken from the daily averages of these CRS data and their spectral indices were calculated as the slopes of the spectra as they would appear on a log-log plot. These results in Figure 3(a) as functions of the time from each V1 and V2 TS crossing show a strong similarity in the time

histories of the V1 and V2 data spectral index values even though the times at V2 are about 2 years and 9 months after the corresponding times at V1. This suggested that distance from the TS was the primary influence on the spectral index values. Figure 3(b) shows the spectral indices as functions of distance from the TS crossing. As V1 was traveling about 1.6 km/s faster than V2 during this period, in the distance plot the V1 line is stretched out farther than in the time plot. This shows that V2 has traveled only a little farther in the heliosheath in 10 years than V1 traveled in 7 years and 9 months.

This dependence on distance from the TS appears consistent with the blunt termination shock model of McComas and Schwadron [16], since as each spacecraft moves into the heliosheath it first traverses field lines that are connected to the TS at increasingly greater distances along the flank of the heliosphere and consequently encounters particles that have received more acceleration. This effect reaches a maximum at about 10 AU beyond the TS, and after that the connection to the acceleration region weakens (though not ending as abruptly as depicted by McComas and Schwadron in [17]). The higher peak spectral index observed at V2 may be related to the fact that the V2 trajectory is at a heliographic inertial longitude of about 217 degrees, while the V1 trajectory is at about 174 degrees, so that V2 is closer in longitude to the acceleration region at 300 or more degrees hypothesized in [17].

4. Particle Behavior Associated with Plasma Wave Events

Another perspective on the particle environment in the LISM (in addition to the simulations discussed in Section 2) and how it may relate to the inward-diffusing particles observed by V2 is provided by the particle behavior associated with the plasma wave events that have been observed in the LISM at around 3 kHz by the V1 Plasma Wave System (PWS). In [10] we discussed how the 3 kHz events that had been observed by V1 up to that time were probably associated with dynamic pressure increases observed by the plasma instrument (PLS) on V2 and with periods of major solar flares, so that solar sources were identified for the merged interaction regions (MIRs) generating the shocks that were discussed by Gurnett et al. [18] as the sources of the PWS events.

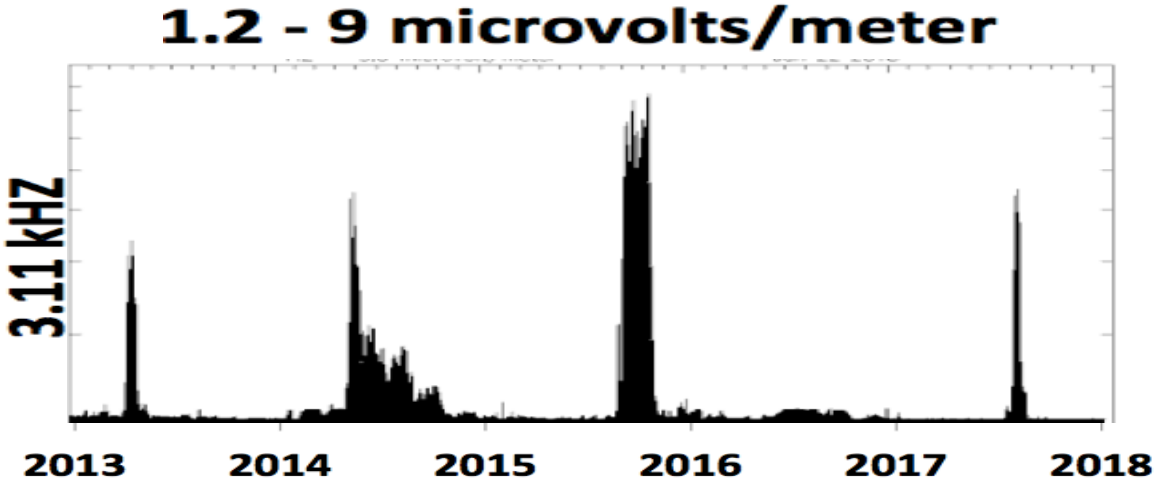

Figure 4. V1 PWS 3.11 kHz channel peak signal in μvolts/m, 2013 through 2017 [19]. The peaks here result from intense electron plasma oscillation events after V1 entered the LISM. The V-shaped dips in the CRS data (Figure 5) extend before and after the PWS events above.

At the time [18] was written only three PWS events had been observed: one in late 2012, one in April and May of 2013, and one that lasted through most of 2014, but the most intense oscillations were in May. Since then, as shown in Figure 4 (which starts at the beginning of 2013, so it omits the event in late 2012; from the University of Iowa website [19]), there have been two more: the strongest one of all in late 2015 and a weaker and much briefer one in August, 2017. As described by Gurnett et al., the data from the PWS broadband analyzer show that the peak frequencies of the plasma wave events have successively increased slightly, indicating slight increases in the plasma density as the spacecraft has travelled more deeply into the LISM, but they all have been within the frequency range

of the 11th channel of the 16-channel analyzer of the PWS. This channel is centered on 3.11 kHz, as indicated in the figure and caption, but actually covers frequencies from about 2.4 to about 4.2 kHz.

Gurnett et al. also discuss the variations of particle count rates associated with the PWS events. The angular resolution of the LECP observations shows that the count rate of the galactic cosmic ray particles gyrating perpendicular to the magnetic field (i.e., with pitch angles near 90 degrees with respect to the field) varies significantly around the times of the PWS events, while the particles moving parallel to the field (i.e., with pitch angles near 0 and 180 degrees) show very little variation. They show in [18] that corresponding variations also appear in the count rate of the guard detector of HET-I in the CRS, although since this detector is omnidirectional it counts particles with all pitch angles, so that the changing count rates of the particles with pitch angles near 90 degrees are superimposed on the nearly constant count rates of the particles with other pitch angles, and hence the percentage changes of the guard count rate are small. Thus, these are more complex phenomena.

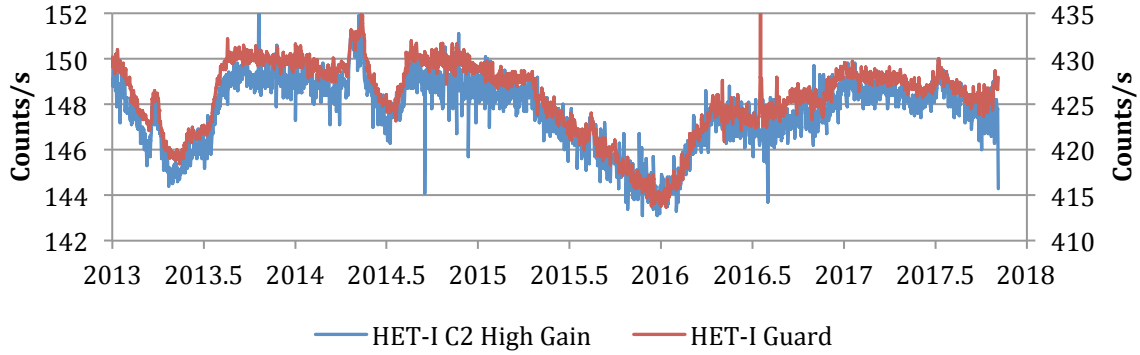

Figure 5. V1 HET-I Detector C2 count rate with no coincidence analysis (left scale) and guard count rate (right scale). The V-shaped dips in Figure 5 correspond to the PWS peaks in Figure 4.

The rates page [11] of the CRS website includes not only count rates for various detector coincidence combinations used in Section 2 but also the rates for individual detectors in the telescopes of the CRS. These individual count rates are unconstrained by coincidence conditions, so they are omnidirectional like the guard count rates, and as exemplified by Figure 5, they show variations associated with the PWS peaks in the same way as the guard count rates. However, Figure 5 is also an example of the smaller count rates from the detectors in the telescope stacks, which are smaller than the cylindrical guard detectors surrounding the telescopes.

In Figure 5 the count rate variations can be seen to have followed the same general pattern for each of the PWS enhancements in Figure 4: a slow decline lasting weeks or months, interrupted by a brief peak, which approximately coincides with the most intense days of the PWS peak, followed by a return to the decline and an eventual bottom, and then a recovery. **Thus in Figure 5, except for each brief peak, the longer-term variation of each count rate resembles a letter V-shaped dip**. However, the pattern was not repeated exactly, since the peaks early in 2013 and in 2014 for the first two events were prominent and the accompanying V-shaped depressions were relatively brief. In contrast, for the third event the V-shaped depression was much deeper and longer-lasting, with a peak barely visible in the figure just after 2015.5. Similarly, for the fourth event the peak was only a little larger than for the third event, and the much shallower depression reached its minimum in the middle of October, about three weeks before the end of the data on November 6.

Gurnett et al. note in the caption to their Figure 3 that the count rate for the guard detector of HET-I is mainly due to protons with energies >20 MeV, but the count rates for the HET detectors provide information about the effects on particles over a wider range of energies. This is because each detector is connected to an amplifier from which the outputs are digitized for the data system, so that each detector has a threshold for the minimum energy of the particles that it detects. Furthermore, in each observation cycle the control system switches the amplifiers between low-gain and high-gain modes.

Thus, plotting the count rates for the HET detectors in each gain mode and taking the ratio between the highest count rate in the peak of the 2014 event and the lowest count rate at the bottom of the depression of the 2015 event provided quantitative measures of the degrees of modulation in a number of energy ranges. Similar degrees of modulation are associated with the PWS events for particles with energies from hundreds of keV to several GeV, so that the most plausible interpretation is that the modulation over all these energies is as described by Gurnett et al., occurring primarily for the particles with pitch angles near 90 degrees, with much less effect on other particles.

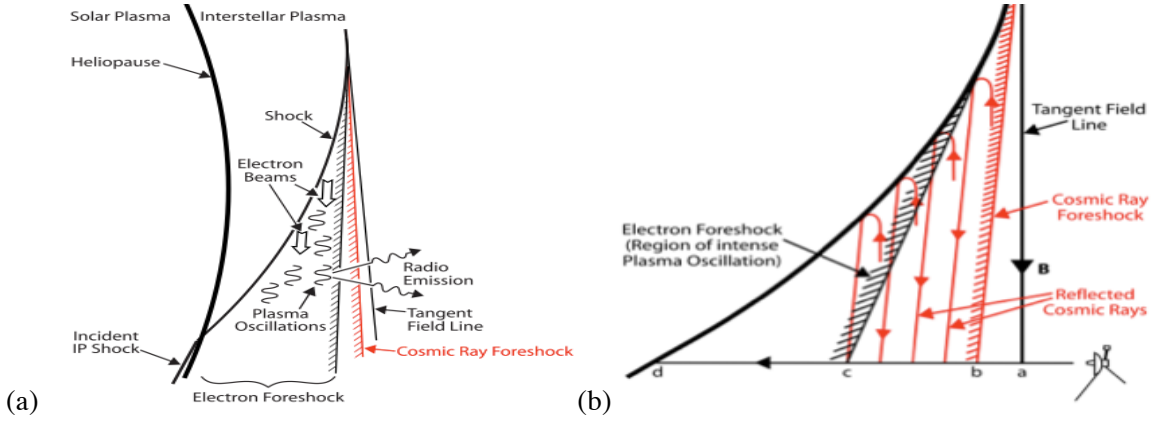

Figure 6. (a) Schematic depiction of the mechanism of plasma wave generation by a beam in the electron foreshock. (b) Schematic depiction of shock motion past the spacecraft and particle peak formation by cosmic ray reflection. (from Figures 7 and 8(a) of [18])

Using an analogy with the bow shock in the solar wind as it collides with the terrestrial magnetosphere, [18] explains the brief peaks in the particle count rates near the times of peak plasma wave intensity. They concluded that this analogy did not provide an explanation for the longer-term V-shaped depressions. They questioned whether the depressions seen near the peaks for the plasma wave events actually were associated with the MIRs for these events, since the depression for the 2013 event started ahead of where the tangent field line could have been, and likewise the depression for the 2012 event began soon after the spacecraft crossed the HP, which also seemed too early to be associated with the shock for that event. They suggest that the depressions are "due to a pre-existing shallow expansion of magnetic field lines draped around the nose of the HP, which via conservation of the first adiabatic invariant would act to decrease the cosmic ray intensities, especially near 90° pitch angles."

Since the particularly broad and deep depression associated with the 2015 event lasted from late winter or early spring of 2015 to early spring of 2016 (so it began about the time the paper was submitted), while V1's solar distance increased from about 130.8 to about 134.5 AU, far beyond the HP crossing at about 121.7 AU, and then the depression for the 2017 event lasted from early 2017 past November 6, from about 138 to over 140 AU, this explanation is no longer plausible. However, the reference to the effect of conservation of the first adiabatic invariant leads to an interpretation consistent with the observations of the more recent plasma wave events as well as the earlier ones.

Figure 6(a) shows Figure 7 of [18] and Figure 6(b) reproduces Figure 8(a) of [18], showing their model of how a shock emerging from the heliosheath generates a cosmic ray foreshock that follows the tangent line to the shock, as shown in Figure 6(a), and an electron foreshock following the cosmic ray foreshock, in which an electron beam generates both the electron plasma oscillations that provide the most intense signals detected by the PWS and also radio signals that propagate ahead of the shock, as were observed in the 2014 event. Figure 6(b) shows how cosmic rays reflected from the shock explain the peak in the count rates near the time when the electron plasma oscillations are observed.

We suggest that the key to understand the V-shaped depressions in the count rates, as shown in Figure 5, is to recognize that the diagrams in Figure 6 represent slices out of the overall 3-dimensional configuration of the moving MIR, representing effects on field lines that are connected to the spacecraft or are close enough to it that the spacecraft is within the gyroradii of many cosmic ray

particles orbiting such field lines with pitch angles near 90 degrees. Figure 7(a) schematically depicts a side view of successive stages of the advance of a shock, taking into account the facts that V1 is at a heliographic inertial latitude of about 34 degrees north, while all the flares that we identified in [10] as likely sources of the MIRs producing the plasma wave events were closer to the solar equator in the northern hemisphere, or were in the southern hemisphere.

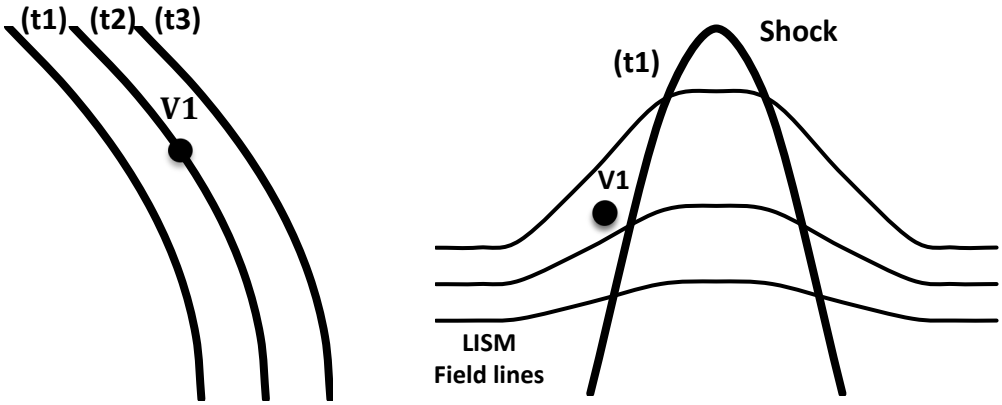

(a) (b)

Figure 7. (a) Schematic depiction of shock profiles at successive times. Horizontal direction is radial and vertical direction is latitude. (b) Schematic depiction of the shock effect on the LISM field at time t_1. Horizontal direction is longitude and vertical direction is radial.

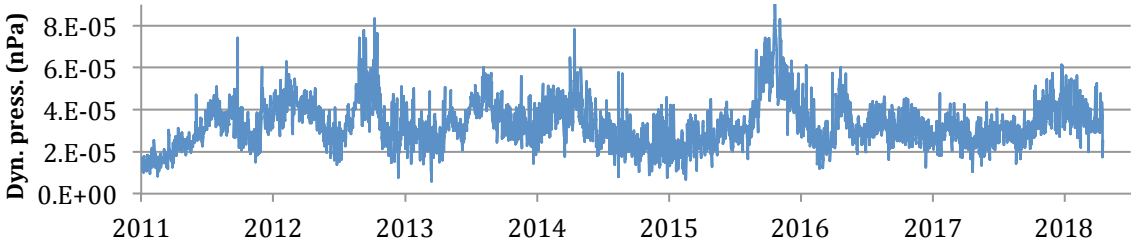

Figure 8. History of PLS plasma dynamic pressures at V2 in nanopascals, from the website in [20].

Thus, at time t_1 the shock has not yet reached V1, but a portion of the shock at lower latitudes has already exceeded the radial distance of V1. At this time the effects depicted in Figure 6 are occurring on field lines too far south of the spacecraft for it to observe them. Time t_2 is the time when the shock reaches the spacecraft and it observes the effects in Figure 6. Then at time t_3 the shock has passed V1 and the effects depicted in Figure 6 are occurring on field lines too far north of the spacecraft for it to observe them and it is also inside the MIR.

However, although at time t_1 the shock has not yet reached the spacecraft, the portion that is already south of the spacecraft would be expected to be deforming the LISM field lines over a wide region. This is schematically depicted in Figure 7(b), showing that V1 would be in a region where the field is being weakened by being stretched by the portion of the shock that is south of the spacecraft, with a corresponding reduction of cosmic ray intensity by conservation of the first adiabatic invariant.

5. Plasma Pressure and Future Prospects

Finally, we consider the hints of possible future developments provided by the recent plasma pressure history at V2. Figure 8 updates Figure 1 from [10], using the file of most recent V2 PLS plasma parameter daily averages from the website in [20]. In addition to the peaks from the middle of 2011 to early 2016 discussed by Richardson, et al. [20], a new pressure peak comparable in magnitude to several of the previous ones has been observed since late 2017. Since magnetometer readings for these recent years are not currently available, it is not known yet if this peak is a MIR like all but the first

two discussed by Richardson, et al., but if so then it may eventually produce another plasma wave event. In any case, activity evidently continues in the outer heliosphere despite declining solar activity.

6. Concluding Remarks

V2 appears to be approaching the HP and may reach it in a few more weeks or months. However, the HP and the LISM just beyond it can be seen from the V1 and V2 observations to be dynamic plasma and particle environments subject to effects propagating from regions not directly observed.

In considering the contrasting results of the modeling efforts reported in [12] and [13], we note that neither used estimates of actual solar wind emission at a source surface a few solar radii from the Sun, as were used by our modeling [10]. They assumed typical values at locations farther from the Sun, as was also done by Washimi et al. [21] for the time after V2 crossed the TS.

We believe comprehensive and consistent understanding of the Voyager observations from great distances in recent years will only come from matching these observations with MHD simulations that include pickup ions and neutral hydrogen and follow the outward propagation of the solar wind actually emitted from the Sun during these times. However, considering the iterative mesh refinements used by Opher et al [12] and by Pogorelov and his collaborators [13], we recognize the great computational challenges of accomplishing the needed simulations. We encourage others to join us in seeking ways to make them feasible.

7. References

[1] Intriligator D S, et al., 2005, *J. Geophys. Res.*, **110**, A09S10
[2] Detman T R, et al., 2011, *J. Geophys. Res.,* **116**, A03105
[3] Intriligator D S, et al., 2012, *J. Geophys. Res.*, **117**, A06104
[4] Intriligator D S, et al., 2015, *J. of Phys. Conf. Ser.* **577**, 012013
[5] Decker R B, et al., 2010, *AIP Conf. Proc.*, **1302**, 51
[6] Stone, E C, et al., 1977, *Space Sci. Rev.*, **21**, 355
[7] Webber W R, and McDonald F B, 2013, *Geophys. Res. Lett.*, **40,** 1665; Stone, E C et al., 2013, *Science*, **341**, 150
[8] Webber W R, and Intriligator D S, 2011, *J. Geophys. Res.*, **116**, A06105
[9] Intriligator D S, et al., 2016, *15th AIAC, "The Science of Ed Stone Celebrating his 80th Birthday:" Journal of Physics Conference Series,* **761**, 012013
[10] Intriligator D S, et al., 2017, *16th AIAC, J. of Phys. Conf. Ser.*, **900,** 105
[11] CRS homepage: https://voyager.gsfc.nasa.gov; rates: https://voyager.gsfc.nasa.gov/rates.html
[12] Opher M, et al, 2011, *Astrophys. J.*, **734**, 71
[13] Pogorelov N, et al., 2017, *Astrophys. J.*, **845**, 9; Borovikov S, et al., 2014, *Astrophys. J. Lett.*, **783**, L16
[14] Roelof E, et al., 2012, *AIP Conf. Proc.*, **1436**, 239. Krimigis S, et al., AGU Fall Mtg, **SH23A-04,** 2016.
[15] Krimigis S M, et al., 2010, 9th AIAC, *AIP Conf. Proc.*, **1302**, 79
[16] McComas D J, and Schwadron N A, 2006, *Geophys. Res. Lett.*, **33**, L04102
[17] McComas D J, and Schwadron N A, 2012, *Astrophys. J.*, **758**, 19
[18] Gurnett D A, et al, 2015, *Astrophys. J.*, **809**, 121
[19] PWS Gurnett and Kurth, http://www-pw.physics.uiowa.edu/das/voyager-pws-sa-list
[20] Richardson J D, et al., 2017, *Astrophys. J.*, **834,** 190;
http://web.mit.edu/afs/athena/org/s/space/www/voyager/voyager_data/voyager_data.html
[21] Washimi H, et al., 2011, *Mon. Not. R. Astron. Soc.*, **416**, 1475

Acknowledgments

We gratefully thank the Voyager projects for the vast information we have received. We acknowledge the support of Carmel Research Center, Inc. We gratefully obtained the: CRS data from [11]; PWS data from Drs. Gurnett and Kurth, and the University of Iowa website [19]; and PLS data from [20].